SHINING LIGHT ON THERMOPHYSICAL NEAR-EARTH ASTEROID MODELING EFFORTS

K. C. Magno, M. C. Kotson, J. D. Ruprecht, J. E. Vaillancourt, and H. E. M. Viggh

MIT Lincoln Laboratory, 244 Wood St, Lexington, MA 02421,
Email: {katrina.magno, michael.kotson, jessica.ruprecht, john.vaillancourt, viggh}@ll.mit.edu

ABSTRACT

Comprehensive thermophysical analyses of Near-Earth Asteroids (NEAs) provide important information about their physical properties, including visible albedo, diameter, composition, and thermal inertia. These details are integral to defining asteroid taxonomy and understanding how these objects interact with the solar system. Since infrared (IR) asteroid observations are not widely available, thermophysical modeling techniques have become valuable in simulating properties of different asteroid types. Several basic models that assume a spherical asteroid shape have been used extensively within the research community. As part of a program focused on developing a simulation of space-based IR sensors for asteroid search, the Near-Earth Asteroid Model (NEATM) developed by Harris, A. in 1998, was selected. This review provides a full derivation of the formulae behind NEATM, including the spectral flux density equation, consideration of the solar phase angle, and the geometry of the asteroid, Earth, and Sun system. It describes how to implement the model in software and explores the use of an ellipsoidal asteroid shape. It also applies the model to several asteroids observed by NASA's Near-Earth Object Wide-field Survey Explorer (NEOWISE) and compares the performance of the model to the observations.

Keywords: Asteroids; Near-Earth Asteroids; NEATM.

1. INTRODUCTION

Near-Earth Asteroid (NEA) impacts of any size have the potential to cause serious geopolitical, environmental, and economic damage. While larger asteroids ($\geq$ 400m) present more hazardous threats, smaller asteroids make up most of the estimated NEA population and are more difficult to observe. In order to predict the consequences of potential impact with the Earth, it is imperative to characterize asteroids based on their physical characteristics. Compared to visible systems, infrared (IR) systems are generally more sensitive to dimmer NEAs [9]. Thermal models have been used extensively to estimate effective diameter, visible albedo, and thermal inertia as well as generate model spectral emitted IR flux densities. They are also used to simulate observations with space-based IR system designs.

This work was part of a larger effort focused on simulating detections of randomly generated NEAs with a variety of sensors. Such a simulation requires a model that can estimate the infrared flux emitted from an asteroid based on its size and thermal properties. The Near-Earth Asteroid Thermal Model (NEATM) [4] was chosen due to its geometric simplicity and consideration of solar phase angles. Its application to several asteroids observed by NASA's Near-Earth Object Wide-field Survey Explorer (NEOWISE) emphasized a need for a comprehensive summary of the model's assumptions. This work also explores the formula changes needed to generalize NEATM for model asteroids with ellipsoidal shapes.

2. NEAR-EARTH ASTEROID THERMAL MODEL (NEATM)

The objective of the model is to estimate the IR flux that is emitted from the illuminated portion of an asteroid and that is visible from Earth. Similar to other thermal models, like the Standard Thermal Model (STM; [6]) and the Fast Rotating Model (FRM; [5]), NEATM assumes the asteroid to be a spherical Lambertian surface and a gray-body emitter. Additionally, the night-side is assumed to emit zero thermal energy, and a calibration factor, the beaming parameter η, is used to account for differences in surface roughness, thermal inertia, beaming effects, and rotation. However, unlike STM, which uses a constant beaming parameter of η=0.756, NEATM iterates through several estimates of η and geometric albedo p_v to minimize a chi-squared fit to observational data. It also considers differences in the solar phase angle α by appropriately adjusting the bounds of the spatial integral of the spectral flux density. Overall, NEATM has been shown to generate more accurate spectral emitted IR flux density estimates than both STM and FRM [3].

2.1. Visual Geometry and Initial Physical Characteristics

Throughout this work, θ and ϕ represent the azimuth and latitude angles, respectively, in a spherical coordinate system centered on the model asteroid. This coordinate system is oriented such that the angular coordinates of the sun are $(\theta, \phi) = (0, 0)$, and the coordinates of the observer are $(\theta, \phi) = (\alpha, 0)$, where the solar phase angle α measures the sun-asteroid-observer angle. Figure 1 illustrates the orientation of the sun, asteroid, and an Earth-based observer in this coordinate system. The hemisphere of the asteroid that is illuminated by the sun spans the azimuth angle range $\theta = [-\pi/2, \pi/2]$ and the latitude angle range $\phi = [-\pi/2, \pi/2]$. The hemisphere visible to the observer spans the same latitude range, but the azimuth range is $\theta = [-\pi/2 + \alpha, \pi/2 + \alpha]$.

Initial guesses of the geometric albedo p_v and beaming parameter η are made to determine the most optimal physical parameter estimates for the specific asteroid through chi-squared fitting. The diameter (D) and bolometric albedo (A) of the asteroid are estimated using the choice of geometric albedo,

$$D = \frac{1329}{\sqrt{p_v}} \tag{1}$$

$$A = qp_v \tag{2}$$

where D is measured in kilometers and q is the visible band phase integral [1].

2.2. Asteroid Temperature Distribution

The temperature distribution function used by NEATM assumes radiative equilibrium at each illuminated point on the surface of the asteroid – energy is conserved since all energy incident on a point is re-radiated from that same point. The emitted flux density of a blackbody can be determined from the temperature T and the Stefan-Boltzmann constant σ through the Stefan-Boltzmann Law.

However, NEATM introduces two extra factors to this relationship. NEATM assumes the asteroid is a graybody, so the emissivity ϵ is needed to describe the total flux emitted relative to a perfect blackbody. We assume $\epsilon = 0.9$ throughout this work. NEATM also uses the beaming parameter η as a calibration factor to correct for the differences in physical characteristics (a perfectly smooth sphere has $\eta = 1$). When implemented into software, a range of η values are iterated over to minimize the chi-square fit, determining the optimal η. Assuming η and ϵ are constant at all points on the asteroid's surface, the emitted flux density Φ_{emitted} at any point on the sphere is

$$\Phi_{\text{emitted}}(\theta, \phi) = \sigma\eta\epsilon\, T^4(\theta, \phi) \tag{3}$$

where $T(\theta, \phi)$ is the temperature of the point on the asteroid's surface located at azimuth θ and latitude ϕ.

The input flux density is dependent on the solar constant S_0 which is the total energy output of the Sun per unit area from a distance of 1 AU. However, some of the input solar radiative energy will be reflected due to the asteroid's bolometric albedo A. By Lambert's cosine law, the absorbed flux at any point is

$$\Phi_{\text{absorbed}}(\theta, \phi) = \frac{S_0(1 - A)\cos(\Psi_S)}{R^2} \tag{4}$$

where R is the sun-asteroid distance in AU, and Ψ_S is the angle between the surface normal at (θ, ϕ) and the vector pointing towards the sun. Using the spherical law of cosines, we can show

$$\cos(\Psi_S) = \cos(\theta)\cos(\phi) \tag{5}$$

Setting Φ_{emitted} equal to Φ_{absorbed} at $(\theta, \phi) = (0, 0)$, where the surface normal points toward the sun, we can derive the subsolar temperature T_{SS}:

$$T_{\text{SS}} = \left[\frac{(1 - A)S_0}{\epsilon\sigma\eta R^2}\right]^{1/4} \tag{6}$$

As the angular distance from the subsolar point increases, the temperature decreases. Furthermore, NEATM defines the temperature of any point on the dark side of the asteroid to be zero. Therefore,

$$T(\theta, \phi) = \begin{cases} T_{\text{SS}}(\cos\theta\cos\phi)^{1/4} & \text{if } \mid \theta \mid \leq \pi/2 \\ 0 & \text{if } \mid \theta \mid > \pi/2. \end{cases} \tag{7}$$

When implemented into software, it is useful to describe equation 7 as

$$T(\theta, \phi) = T_{\text{SS}}(\max(0, \cos\phi\cos\theta))^{1/4} \tag{8}$$

2.3. Emitted IR Flux Density

NEATM allows us to estimate the radiation, emitted from the illuminated portion of the asteroid, that is visible to the observer. Because the model assumes that the asteroid is a graybody emitter, the spectral irradiance at any point on the surface can be described using Planck's function:

$$B_\lambda(T(\theta, \phi)) = \frac{2hc^2/\lambda^5}{\exp(hc/\lambda kT) - 1} \tag{9}$$

where λ is the wavelength of radiation and T is the temperature as defined by equation 8. The total flux with wavelength λ emitted toward the observer is

$$F_\lambda = \epsilon \int_h B(\lambda, T(\theta, \phi))\cos(\Psi) d\Omega \tag{10}$$

The flux is integrated over h, the hemisphere of the asteroid visible to the observer, and $d\Omega$ is the differential solid

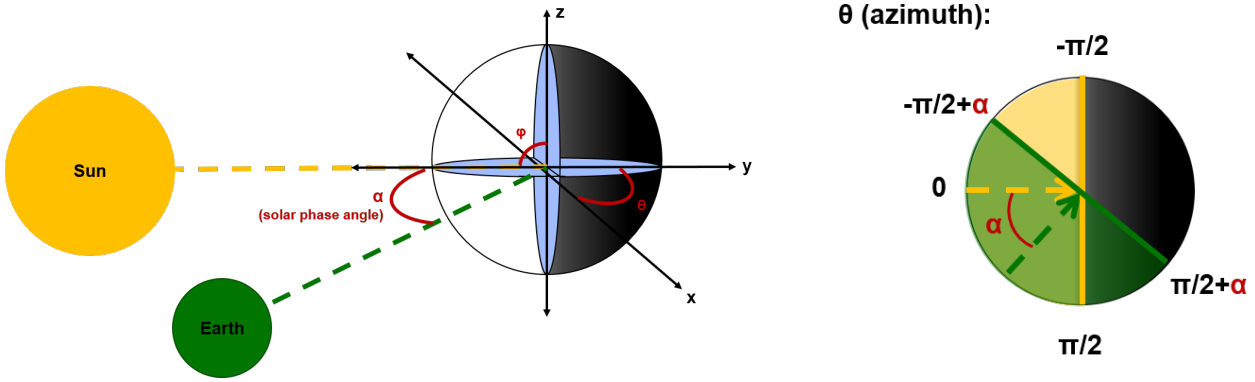

(a) (b)

Figure 1: Explanation of the model coordinate axes (a) and the view of the model asteroid from above its north pole (b). The yellow and green arrows represent the sun-asteroid and observer-asteroid vectors, respectively. The light-green area in (b) shows the portion of the asteroid that is both illuminated by the sun and visible to the observer.

angle. Ψ is the angle between the surface normal at the point (θ, ϕ) and the vector pointing towards the observer. Using the spherical law of cosines to find the angle between (θ, ϕ) and $(\alpha, 0)$, we can derive

$$\cos(\Psi) = \cos(\phi)\cos(\theta - \alpha) \tag{11}$$

Then, using the definition $d\Omega = \cos(\phi)d\theta\, d\phi$, we arrive at

$$F_\lambda = \epsilon \iint B(\lambda, T(\theta, \phi)) \cos^2(\phi) \cos(\theta - \alpha) d\theta\, d\phi \tag{12}$$

The geocentric distance Δ and the asteroid diameter D are added to the observed flux density equation through the inverse square law. We define the hemisphere h as the integral bounds $[-\pi/2, \pi/2]$ for ϕ and $[-\pi/2 + \alpha, \pi/2 + \alpha]$ for θ (see Figure 1). Due to symmetry, we can change the bounds on ϕ to $[0, \pi/2]$ and introduce a factor of 2:

$$F_{\lambda,\text{obs}} = \frac{2\epsilon(\frac{D}{2})^2}{\Delta^2} \int_0^{\frac{\pi}{2}} \int_{-\frac{\pi}{2}+\alpha}^{\frac{\pi}{2}+\alpha} \frac{2hc^2\lambda^{-5}}{\exp(hc/\lambda kT) - 1} \times \cos^2\phi \cos(\theta - \alpha) d\theta\, d\phi \tag{13}$$

Thus, the observed spectral IR flux density (in units of $\text{W/m}^2/\mu\text{m}$) emitted by the model asteroid is

$$F_{\lambda,\text{obs}} = \frac{\epsilon D^2}{\Delta^2} \int_0^{\frac{\pi}{2}} \int_{-\frac{\pi}{2}+\alpha}^{\frac{\pi}{2}+\alpha} \frac{hc^2\lambda^{-5}}{\exp(hc/\lambda kT) - 1} \times \cos^2\phi \cos(\theta - \alpha) d\theta\, d\phi \tag{14}$$

3. VALIDATING THE NEATM IMPLEMENTATION

We planned to use our software implementation of NEATM to generate flux values for a random ensemble of asteroids as part of a simulated NEA observation campaign. To test that our code was providing accurate fluxes for the simulation, we followed the validation methods outlined in [7], applying our model to well-studied asteroids and comparing the results against photometry from the WISE mission. We focused this analysis on the W1 and W2 WISE bands (3.4 μm and 4.6 μm, respectively), so that we could test how accurately our software calculates both emitted and reflected IR light.

For our validation tests we selected 13 objects from Table 1 of [7] with diameters between 80 and 280 km. We obtained a list of WISE observations for each object using the Catalog Search tool of the NASA/IPAC Infrared Science Archive (IRSA[1]). We queried for observations using the "All Sky Search" option of the WISE All-Sky Known Solar System Object Possible Association List, obtaining between 10 and 25 unique observations for each object. Each observation included values for the object's distances from the sun and earth, solar phase angle, and magnitude across the WISE photometric bands at a specific time. We discarded any observations for which no W1 or W2 magnitudes were available and those with outlier magnitude values.

Using the distance and phase angle information from IRSA and the diameter, albedo, and beaming parameter values listed for each object in [7], we used our NEATM implementation to simulate each observation. To compare our flux calculations against WISE photometry, it was necessary to apply color correction factors. Flux correction factors for each WISE passband are listed in [10] for a variety of spectral types. The correction factors for thermally emitted infrared light are quite significant at temperatures less than 400 K. As such, we adjusted our NEATM function from equation 14 to be the following:

[1] https://irsa.ipac.caltech.edu/Missions/wise.html

$$F_\lambda = \frac{\epsilon D^2}{\Delta^2} \int_0^{\pi/2} \int_{-\pi/2+\alpha}^{\pi/2+\alpha} f_c(\lambda, T) \frac{hc^2\lambda^{-5}}{\exp(hc/\lambda kT) - 1} \times \cos^2\phi \cos(\theta - \alpha) d\theta \, d\phi \quad (15)$$

where $f_c(\lambda, T)$ is the color correction factor for the W1 or W2 bandpass at the given temperature. We used linear interpolation and extrapolation to obtain the value of f_c for any value of T not listed in the reference.

For infrared light *reflected* off an asteroid, which has the same spectral shape as the light emitted from the sun, the correction factor is less than 2%. The reflected flux is calculated according to the methods outlined in [8], using the infrared albedos listed in [7] and the visible light HG phase function [1].

After combining the reflected and color-corrected emitted flux for each simulated observation, we converted the fluxes into W1 and W2 magnitudes using the photometric zero points of 8.180×10^{-15} and 2.415×10^{-15} W/cm^2/μm for the W1 and W2 bandpasses, respectively [10].

Figure 2 shows how our model photometry compares to the WISE photometry in both the W1 and W2 bands for the selected asteroids. The error bars for each data point are due solely to the variance in measured WISE magnitudes across all observations of the given object. Uncertainty values for each object's diameter, albedo, and beaming parameter, are listed in [7], but we have not yet integrated these values into our error analysis. As such, we expect that the errors in Figure 2 are currently underestimated for both the individual objects and the overall average.

It is clear from Figure 2 that our implementation of the NEATM algorithm computes flux values that – on average – are within error of observed photometry. There are significant outliers that may warrant further investigation (such as 22 Kalliope and 31 Euphrosyne), but we expect that our software can model the infrared flux of a large ensemble of synthetic asteroids without any significant systematic inaccuracies.

4. ELLIPSOIDAL NEATM

While NEATM is useful for estimating the sizes and thermal properties of asteroids, it is perhaps limited in its assumption that the target asteroid is spherical. Prior work by Robert Brown [2] expanded the Standard Thermal Model to the more general case of a triaxial ellipsoidal asteroid. Following in those footsteps, we derived an ellipsoidal variant of NEATM and explored its applicability towards current NEA research.

We begin by defining our model asteroid as a triaxial ellipsoid with semi-major axes of length a, b, and c aligned with the x, y, and z body axes, respectively:

$$\frac{x^2}{a^2} + \frac{y^2}{b^2} + \frac{z^2}{c^2} = 1 \quad (16)$$

By taking the gradient of the above equation, we can find the normal vector $\vec{N}(x, y, z)$ at any point on the surface.

$$\vec{N}(x, y, z) = \frac{2x}{a^2}\hat{x} + \frac{2y}{b^2}\hat{y} + \frac{2z}{c^2}\hat{z} \quad (17)$$

To simplify our integration at later steps, it will be useful to describe the ellipsoid and its surface normal vectors in spherical coordinates. We define the latitude ϕ such that $\phi = \pi/2$ along the z-axis and the azimuth θ such that $\theta = 0$ along the x-axis. At any point on the surface of the ellipsoid described by (θ, ϕ), the radial distance from the origin r is thus

$$r = \left(\frac{\cos^2\theta \cos^2\phi}{a^2} + \frac{\sin^2\theta \cos^2\phi}{b^2} + \frac{\sin^2\phi}{c^2} \right)^{-1/2} \quad (18)$$

As described in [2], the observable flux emitted at any point on the asteroid's surface is determined by the surface normal vector, the vector pointing at the sun, and the vector pointing at the observer. Because the magnitudes of the asteroid-observer and asteroid-sun vectors are much larger than the size of the asteroid, we can translate each surface normal $\vec{N}$ so that its tail begins at the origin of the body axes instead of at the ellipsoid's surface. This allows us to describe $\vec{N}$ in terms of θ_N and ϕ_N, the azimuthal and altitudinal orientation of the surface normal with respect to the spherical body axes:

$$\theta_N(\theta, \phi) = \arctan\left(\frac{a^2}{b^2} \tan\theta \right) \quad (19)$$

$$\phi_N(\theta, \phi) = \operatorname{arccot}\left(c^2 \cot\phi \sqrt{\frac{\cos^2\theta}{a^4} + \frac{\sin^2\theta}{b^4}} \right) \quad (20)$$

where θ and ϕ are the spherical coordinates of the point on the ellipsoid corresponding to the surface normal. Finally, we define two more unit vectors, one pointing towards the observer in the body axes, and the other pointing towards the sun. As with the normal vectors, we can describe the orientation of these vectors as (θ_O, ϕ_O) for the observer and (θ_S, ϕ_S) for the sun. Even if the orientation of the asteroid's body axes with respect to the sun and the observer is unknown, we still know that the angle between the sun and observer vectors must be equal to the phase angle, α. Using the spherical law of cosines,

$$\cos\alpha = \sin\phi_O \sin\phi_S + \cos\phi_O \cos\phi_S \cos(\theta_O - \theta_S) \quad (21)$$

Now we can find the temperature at every point on the surface of the ellipsoid. The subsolar temperature T_{SS} is still calculated using equation 8. This is the temperature of the point on the ellipsoid where the surface normal

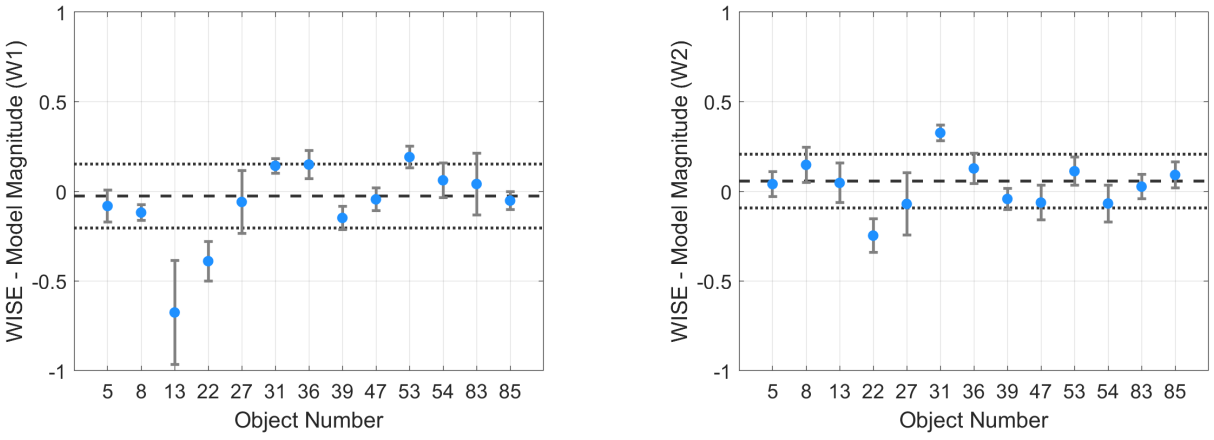

Figure 2: Model magnitudes versus WISE photometry for W1 (a) and W2 (b) bands. Blue dots show the average difference between model magnitude and WISE magnitude for each asteroid. Error bars show the standard deviation of the differences due to variation in the observed magnitudes. The dashed line shows the weighted mean difference across all objects, and the dotted lines are 1σ error bounds on the weighted mean.

points toward the sun ($\theta_N = \theta_S$ and $\phi_N = \phi_S$). The temperature of every other point on the surface decreases as the normal vector points away from the sun:

$$\mu_S(\theta,\phi) = \sin\phi_N \sin\phi_S + \cos\phi_N \cos\phi_S \cos(\theta_N - \theta_S) \tag{22}$$

$$T(\theta,\phi) = T_{\mathrm{SS}}(\max(0,\mu_S))^{1/4} \tag{23}$$

where μ_S is the cosine of the angle between the surface normal at (θ,ϕ) and the solar vector, calculated using the spherical law of cosines. Note that, just as in the spherical formulation of NEATM, the temperature of any point on the surface pointing away from the sun is defined to be zero.

Because we are modeling the ellipsoidal asteroid as a graybody emitter, we can now use the Planck function to find the flux emitted from each point on the surface. The fraction of that flux emitted towards the observer μ_O is equal to the cosine of the angle between the surface normal and the observer vector:

$$\mu_O(\theta,\phi) = \sin\phi_N \sin\phi_O + \cos\phi_N \cos\phi_O \cos(\theta_N - \theta_O) \tag{24}$$

Finally, we integrate the flux contributions over the entire surface of the ellipsoid to obtain $F_{\mathrm{NEATM,Ellipsoid}}$, the monochromatic flux density emitted by the model asteroid:

$$F_{\mathrm{NEATM,Ellipsoid}} = \frac{\epsilon}{\Delta^2} \int_0^{2\pi} \int_{-\pi/2}^{\pi/2} B_\lambda(T(\theta,\phi)) \times \max(0,\mu_O) r^2 \cos\phi \, d\phi \, d\theta \tag{25}$$

where Δ is the distance between the asteroid and the observer. Note that we integrate over the entire range of spherical coordinates, not just a hemisphere as in equation 14. This is because defining integral limits such that $\mu_O \geq 0$ is non-trivial in the body axis coordinate system we've chosen.

At first glance, this ellipsoidal variant of NEATM seems to add too many fitting parameters to be useful. Spherical NEATM can be fit to coarse IR spectroscopy to derive the asteroid's beaming parameter and diameter; the ellipsoidal model requires two extra size parameters (a, b, and c versus D) and three angular parameters describing the asteroid's orientation. However, the ellipsoidal model may prove more helpful if any of these extra parameters can be constrained. If an asteroid has large rotational light curve variatons, for instance, then we could make the assumption that the maximum/minimum points on the curve are when the largest/smallest possible cross sections are visible to the observer. This would require that one of the body axes is aligned with the viewer's line of sight, constraining two of the angular parameters describing the body's orientation. Further research is necessary to determine how the ellipsoidal NEATM would affect best-fit beaming parameters (compared to spherical NEATM) in these scenarios.

REFERENCES

1. Bowell E., Hapke B., Domingue D., et al., (1989). Application of photometric models to asteroids, In *Asteroids II*, 524-556.
2. Brown R., (1985). Ellipsoidal geometry in asteroid thermal models: The standard radiometric model, *Icarus*, **64**(1), 53-63.
3. Delbó M. and Harris A., (2002). Physical properties of near-Earth asteroids from thermal infrared observations and thermal modeling, *Meteoritics & Planetary Science*, **37**(12), 1929-1936.
4. Harris A. W., (1998). A Thermal Model for Near-Earth Asteroids, *Icarus*, **131**(2), 291-301.

5. Lebofsky L. A., Veeder G. J., Lebofsky M. J., et al., (1978). Visual and radiometric photometry of 1580 Betulia, *Icarus*, **35**(3), 336-343.

6. Lebofsky L. A., Sykes M. V., Tedesco E. F., et al., (1986). A refined "standard" thermal model for asteroids based on observations of 1 Ceres and 2 Pallas, *Icarus*, **68**(2), 239-251.

7. Mainzer A., Grav T., Masiero J., et al., (2011). Thermal model calibration for minor planets observed with wide-field infrared survey explorer/NEOWISE, *The Astrophysical Journal*, **736**(2), 100.

8. Myhrvold N., (2018). Asteroid thermal modeling in the presence of reflected sunlight, *Icarus*, **303**, 91-113.

9. Stokes G., Barbee B., Bottke W., et al., (2017). Update to determine the feasibility of enhancing the search and characterization of NEOs, *Technical Report*, Prepared by the Near-Earth Object Science Definition Team at the request of NASA.

10. Wright E., Eisenhardt P., Mainzer A., et al., (2010). The Wide-field Infrared Survey Explorer (WISE): mission description and initial on-orbit performance, *The Astrophysical Journal*, **140**(6), 1868.

ACKNOWLEDGMENTS

This material is based upon work supported by the National Aeronautics and Space Administration (NASA) under Air Force Contract No. FA8702- 15-D-0001. The views, opinions, and/or findings expressed are those of the author(s) and should not be interpreted as representing the official views or policies of the U.S. Government. Distribution A. Approved for public release - distribution is unlimited.